

# Theoretical analysis for heat exchange performance of transcritical nitrogen evaporator used for liquid air energy storage

Yu, Qinghua; Song, Wenji; Al-Duri, Bushra; Zhang, Yan; Xie, Danmei; Ding, Yulong; Li, Yongliang

DOI:

[10.1016/j.applthermaleng.2018.06.028](https://doi.org/10.1016/j.applthermaleng.2018.06.028)

License:

Creative Commons: Attribution-NonCommercial-NoDerivs (CC BY-NC-ND)

*Document Version*

Peer reviewed version

*Citation for published version (Harvard):*

Yu, Q, Song, W, Al-Duri, B, Zhang, Y, Xie, D, Ding, Y & Li, Y 2018, 'Theoretical analysis for heat exchange performance of transcritical nitrogen evaporator used for liquid air energy storage', *Applied Thermal Engineering*, vol. 141, pp. 844-857. <https://doi.org/10.1016/j.applthermaleng.2018.06.028>

[Link to publication on Research at Birmingham portal](#)

## **Publisher Rights Statement:**

Checked for eligibility: 28/06/2018

<https://doi.org/10.1016/j.applthermaleng.2018.06.028>

## **General rights**

Unless a licence is specified above, all rights (including copyright and moral rights) in this document are retained by the authors and/or the copyright holders. The express permission of the copyright holder must be obtained for any use of this material other than for purposes permitted by law.

- Users may freely distribute the URL that is used to identify this publication.
- Users may download and/or print one copy of the publication from the University of Birmingham research portal for the purpose of private study or non-commercial research.
- User may use extracts from the document in line with the concept of 'fair dealing' under the Copyright, Designs and Patents Act 1988 (?)
- Users may not further distribute the material nor use it for the purposes of commercial gain.

Where a licence is displayed above, please note the terms and conditions of the licence govern your use of this document.

When citing, please reference the published version.

## **Take down policy**

While the University of Birmingham exercises care and attention in making items available there are rare occasions when an item has been uploaded in error or has been deemed to be commercially or otherwise sensitive.

If you believe that this is the case for this document, please contact [UBIRA@lists.bham.ac.uk](mailto:UBIRA@lists.bham.ac.uk) providing details and we will remove access to the work immediately and investigate.

1

2

3

4

5

6       **Theoretical analysis for heat exchange performance of**

7       **transcritical nitrogen evaporator used for liquid air energy**

8                               **storage**

9

10

11

12       Qinghua Yu<sup>a,b</sup>, Wenji Song<sup>c</sup>, Bushra Al-Duri<sup>a</sup>, Yan Zhang<sup>a</sup>, Danmei Xie<sup>b</sup>, Yulong Ding<sup>a</sup>,

13                               Yongliang Li<sup>a,\*</sup>

14

15

16

17       <sup>a</sup> Birmingham Centre for Energy Storage, School of Chemical Engineering, University of

18                               Birmingham, Birmingham B15 2TT, United Kingdom

19       <sup>b</sup> School of Power and Mechanical Engineering, Wuhan University, Wuhan 430072, China

20       <sup>c</sup> Guangzhou Institute of Energy Conversion, Chinese Academy of Sciences, Guangzhou

21                               510640, China

---

\*Corresponding author. Tel.: [REDACTED], Email: [y.li.1@bham.ac.uk](mailto:y.li.1@bham.ac.uk) (Y. Li)

## Abstract

In view of violent changes of thermo-physical properties, the segmental design method is adopted to explore the heat exchange performances of the transcritical nitrogen (T-N<sub>2</sub>) evaporator used for liquid air energy storage, in which cold N<sub>2</sub> is heated up successively by hot propane and methanol in two wide temperature sections. The local heat capacity rate ratio between cold and hot fluids has crucial effects on the local heat exchange performance of evaporator, such as local effectiveness, local entransy dissipation, and local required heat conductance or local heat transfer rate. They have extremums near the positions where the local heat capacity rate ratio equals one, but their optimal values need to be determined by combining the changing trend of the local heat capacity rate ratio. The total heat exchange performance of evaporator is evaluated using total entransy dissipation and total exergy efficiency. When the heat load is fixed, the total performance is improved with the decrease in the mass flow rate of methanol, but at the expense of the required total heat conductance; The total performance can be optimized by precisely tailoring the heat load ratios between the two temperature sections. When the heat conductance is given, the optimum total performance can be obtained by adjusting the mass flow rate of hot fluids at a fixed heat conductance ratio; Increasing the heat conductance ratio of the low temperature section can further elevate the optimum total performance whereas the affordable heat load or the outlet temperature of N<sub>2</sub> is notably decreased. Increasing N<sub>2</sub> pressure elevates the total performance of evaporator but diminishes the extractable cold amount from the liquid N<sub>2</sub> in the same temperature rise. This work is beneficial for selection of key parameters to achieve optimal operation of the T-N<sub>2</sub> evaporator.

*Keywords:* Heat exchanger; Supercritical nitrogen; Entransy dissipation; Exergy efficiency; Energy storage.

## Nomenclature

### Roman letters

$c_p$	specific heat ( $\text{J} \cdot \text{kg}^{-1} \cdot \text{K}^{-1}$ )
$D_{\text{re}}$	relative difference
$\dot{E}_{\text{dis}}$	entransy dissipation ( $\text{W} \cdot \text{K}$ )
$EX$	flow exergy ( $\text{W}$ )
$h$	specific enthalpy ( $\text{J} \cdot \text{kg}^{-1}$ )
$HA$	heat conductance ( $\text{W} \cdot \text{K}^{-1}$ )
$m$	mass flow rate ( $\text{kg} \cdot \text{s}^{-1}$ )
$mc_p$	heat capacity flow rate ( $\text{W} \cdot \text{K}^{-1}$ )
$M$	number of sub-heat exchangers in the low temperature section
$N$	number of all sub-heat exchangers
$Ntu$	number of heat transfer units
$P$	pressure ( $\text{Pa}$ )
$q$	local heat transfer rate ( $\text{W}$ )
$Q_{\text{tot}}$	total heat load ( $\text{W}$ )
$R_c$	the ratio between the smaller and bigger heat capacity flow rates
$R_{c,hc}$	the ratio of heat capacity rate of hot fluid to that of cold fluid
$s$	specific entropy ( $\text{J} \cdot \text{kg}^{-1} \cdot \text{K}^{-1}$ )
$T$	temperature ( $\text{K}$ )

### Greek letters

$\varepsilon$	effectiveness
$\eta_{EX}$	exergy efficiency
$\tau$	the ratio of heat load in the low temperature section to that in the whole evaporator
$\varphi$	the ratio of heat conductance in the low temperature section to that in the whole evaporator

### Subscripts

0	environmental conditions
$c$	cold fluid
$h$	hot fluid
$hl$	hot fluid in the low temperature section
$hh$	hot fluid in the high temperature section
$i$	inlet
$j$	local position
$m$	mean value
$o$	outlet

## 1. Introduction

Liquid air energy storage (LAES) as a promising solution for grid scale energy storage has attracted much attention in recent years [1-5]. The LAES uses liquid air/nitrogen ( $N_2$ ) as both storage medium and working fluid for charging and discharging processes of electrical energy. During the charging process, excess or cheapest electricity drives air liquefaction and separation plants to produce liquid  $N_2$  stored in cryogenic tanks at the nearly atmospheric pressure. During the discharging process, the liquid  $N_2$  is first pressurized by a cryogenic pump and then heated up to expand in turbines to generate electricity. Cold thermal energy released in preheating of liquid  $N_2$  during the discharging process can be captured to lessen refrigeration load of air liquefaction during the charging process. In view of time mismatch of the charging and discharging processes, the captured cold thermal energy required to be stored. Such a design of cold recycle based on cold storage in LAES significantly improves the overall system efficiency [2]. Conventionally, cold storage is implemented using packed beds of pebbles or rocks operating at nearly atmospheric pressure [6-8]. Operating experience of a 350 kW/2.5 MWh pilot plant located at the University of Birmingham manifested that the temporary cold storage using packed beds results in round trip efficiency improvement of LAES by ~50%. However, the dynamic effects in packed beds caused by thermal front propagation can lead to an undesired increase by 25% in the energy consumption of air liquefaction [9]. Therefore, it is required to design a novel high-efficiency cold storage unit.

Similar to sensible heat storage using liquids as medium, Li et al. [10] proposed a cold storage unit based on combination of two thermal fluids, which were used as both heat transfer fluids and cold storage mediums. Both She et al. [11] and Pen et al. [12] also adopted the same cold storage unit in their proposed novel LAES system. The reason for adopting two thermal fluids is that no single fluid can work totally in the form of its liquid state in the wide working temperature range of the liquid  $N_2$  preheating process. The two fluids are propane

and methanol selected owing to their suitable working temperate ranges and comparatively large heat capacity [10]. A two-tank configuration was designed for each of the two fluids to recover and store cold energy, which can realize quasi-steady heat transfer in heat exchangers to overcome dynamic effects in packed beds [13]. The proposed unit can notably simplify the LAES system involving cold storage and offer more straightforward and flexible operating strategy with respect to the conventional packed beds [10]. The calculations indicated that the selected thermal fluids exhibit higher volume-based energy storage density than pebbles or concrete [10, 14]. This implies that a more compact system can be obtained by using the selected fluids as cold storage mediums.

The discharging pressure, namely the inlet pressure of the first stage turbine, is one of major operating parameters influencing the performance of LAES system. With the increase in the discharging pressure, the resulting specific expansion work increases while the recyclable cold amount diminishes [9]. In order to increase the output power of turbines, the liquid  $N_2$  is generally pressurized above the critical pressure of  $N_2$  before the inlet of first stage turbine [9, 13]. Thus  $N_2$  will undergo phase transition from the liquid state to the supercritical state in the liquid  $N_2$  preheating process. For convenience, this phase transition is also called evaporation similar to liquid-gas phase transition, and the corresponding heat exchanger is named transcritical  $N_2$  (T- $N_2$ ) evaporator in the present paper. The performance of the evaporator determines the amount of recovered cold and the inlet temperature of turbines in a LAES system, and thus has crucial influences on the operation efficiency and stability of the system [9]. However, the thermodynamic properties of  $N_2$  change dramatically around the pseudo-critical temperature, which makes the heat transfer in the evaporator rather complicated and the design of the evaporator very challenging.

Some studies have been devoted to the heat transfer characteristics of supercritical  $N_2$  [15-19]. Dimitrov et al. [15] conducted experiments on forced convective heat transfer of

supercritical nitrogen at a pressure of 4 MPa in a vertical tube. The results indicated that the heat transfer can be enhanced when the difference between wall and bulk temperatures spans the drastic variation region of the thermo-physical properties of N<sub>2</sub>. Zhang et al. [17] carried out experimental and numerical studies on flow and heat transfer of supercritical N<sub>2</sub> in a vertical mini-tube. They reported that there is considerable discrepancy in Nusselt numbers between the experimental results and the predictions by the existing correlations. Ciprian et al. [19] numerically examined the heat transfer coefficient of supercritical N<sub>2</sub> in the large specific heat region flowing upward in a vertical tube under different operating pressures. They found that the increase of heat flux could cause heat transfer deterioration. The above studies almost focus on the heat transfer behaviours of supercritical N<sub>2</sub> under fixed heat flux conditions. Actually, the heat transfer in the evaporator is coupled between the N<sub>2</sub> and the transfer fluids, and hence the heat transfer condition of N<sub>2</sub> is changing along the flow direction of N<sub>2</sub>. Therefore, deep understanding of coupled the heat transfer behaviours between N<sub>2</sub> and two heat transfer fluids in the evaporator is crucial to the optimization design of evaporator for improving performances of the LAES system.

From the above, although such a T-N<sub>2</sub> evaporator including the combination of propane and methanol as heat transfer fluids has been adopted by several researches [10-12], studies available in the literature have not addressed the following key aspects: (1) the local and overall heat exchange performances of the evaporator coupled with three fluids in the case of drastic change of the thermo-physical properties of N<sub>2</sub>; (2) how to select the key operating parameters, including mass flow rates of heat transfer fluids, inlet pressure of N<sub>2</sub>, and heat load or conductance distribution ratio between the two heat transfer fluids. Therefore, this paper adopts the segmental design method [20] to precisely capture the coupled heat transfer behaviours in the T-N<sub>2</sub> evaporator, and employs the entransy dissipation theory [21] and exergy analysis method [22] to evaluate the heat exchange performance of the evaporator.

The local performances of the evaporator as well as its overall performances are explored in detail from the respective viewpoints of design and check calculations. The effects of the key operating parameters on the entransy dissipation, exergy efficiency, and required heat conductance or affordable heat load of the evaporator are examined for optimization of these parameters. This study can provide significant references for optimization of T-N<sub>2</sub> evaporator to achieve high-efficiency cold storage in the LAES system.

## 2. Theoretical approach

### 2.1. Segment design and main assumptions

The critical point of N<sub>2</sub> locates at (126.19 K, 3.4 MPa). Fig.1 shows variation of the specific heat of N<sub>2</sub> with temperature above critical pressures. It is evident that the specific heat exhibits severe change near pseudo-critical point, which is beneficial to extracting more cold energy, but makes the heat exchanger design more difficult than fixed properties. According to the respective working temperature ranges of the selected two heat transfer fluids, the evaporator is artificially divided into a low temperature section for propane and a high temperature section for methanol. The two hot fluids are used to successively heat up the cold fluid N<sub>2</sub> [10-12]. Based on the segment design method as mentioned above, the evaporator with counter-flow configuration is discretized into a sufficient number of serial sub-heat exchangers (SHEs) as depicted in Fig. 2 [20, 23], where  $T$  denotes the temperature;  $q$  indicates the local heat transfer rate; subscripts  $c$  and  $h$  denote the cold and hot fluids, respectively; subscript  $j$  indicates the local position; subscripts  $hl$  and  $hh$  indicate the hot fluids in the low and high temperature sections, respectively; subscripts  $i$  and  $o$  denote inlet and outlet, respectively;  $N$  and  $M$  represent the numbers of SHEs in the whole evaporator and the low temperature section, respectively.  $M$  can be calculated by  $M = \tau N$  for design calculation or  $M = \varphi N$  for check calculation, where  $\tau$  and  $\varphi$  represent the ratios of heat load



and heat conductance in the low temperature section to those in the whole evaporator, respectively. An equality of temperature exists at the junction of each two SHEs for the cold and hot fluids, respectively.

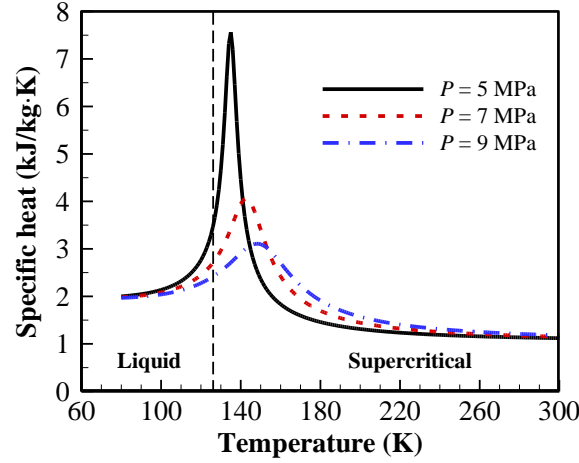


Fig. 1. The specific heat of  $N_2$  dependent on temperature at pressures of 5 MPa, 7 MPa and 9 MPa.

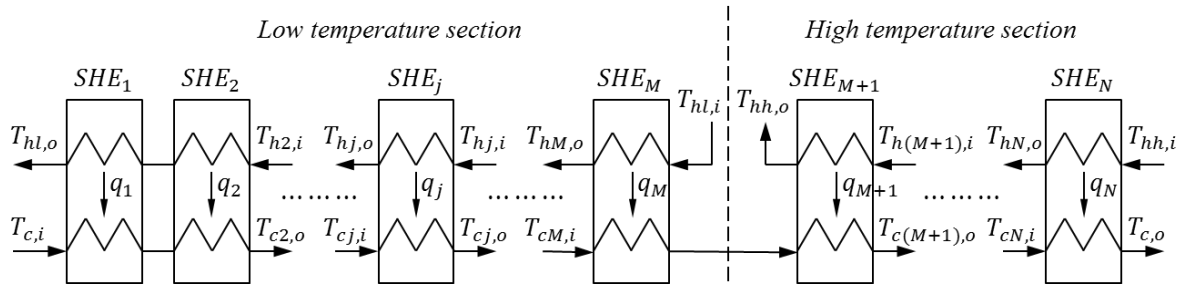


Fig. 2. The schematic diagram of SHEs for three types of fluids.

In order to formulate the heat exchange problem in a T- $N_2$  evaporator, the following assumptions were made: (a) the specific heats of cold and hot fluids are considered to be constant in each SHE as the evaporator is divided into enough number of SHEs; (b) the heat transfer coefficient is considered to be invariable in each SHE as the number of SHEs is enough; (c) there is no heat or cold loss from the evaporator to environment due to good thermal insulation layers on the outer surfaces of evaporator; (d) the heat conduction along axial direction in heat transfer surface of the evaporator is negligible since the thickness of heat transfer surface of the evaporator is quite small compared to its axial length; (e) the pressure drop of cold and hot fluids caused by flow friction is ignorable considering that the

pressure drop by flow friction is very small compared to the inlet pressure and has tiny influences on the thermo-physical properties of fluids; (f) for the sake of ensuring the continuity of heat exchange and avoiding heat exchange between the two hot fluids, it is assumed that the inlet temperature of the hot fluid in the low temperature section is equal to the outlet temperature of the hot fluid in the high temperature section, i.e.  $T_{hl,i} = T_{hh,o}$ . This constraint condition can easily be achieved by reasonable design; (g) a safe temperature difference of 5 K, with respect to the freezing point or boiling point of each hot fluid, is specified to ensure that each hot fluid operates at the liquid state in the evaporator. The proposed safe temperature difference of 5 K is enough for avoiding freezing or boiling of hot fluids caused by occasional temperature fluctuation, and it is not too large to markedly narrow the optional range of mass flow rates of hot fluids. As a result of the assumptions (a-d), the effectiveness—number of heat transfer unit ( $\epsilon - NTU$ ) method is applicable for each SHE [23].

## 2.2. Basic equations based on segment design method

For the design calculation, the total heat load of evaporator denoted by  $Q_{tot}$  is fixed, which can be determined by the given mass flow rate, inlet and outlet statuses of  $N_2$  as follows:

$$Q_{tot} = m_c(h_{c,o} - h_{c,i}), \quad (1)$$

where  $m$  is the mass flow rate of fluid and  $h$  is the specific enthalpy. The specific enthalpies are totally dependent on the given temperatures and pressures at the inlet and outlet of  $N_2$ .

It is prescribed that the total heat load is evenly divided among the SHEs, and thus the local heat transfer rate of each SHE can be calculated by  $q_j = Q_{tot}/N$ . According to the definition, the local effectiveness of each SHE can be written as [24]

$$\varepsilon_j = \frac{q_j / \min(m_c c_{pj,c}, m_h c_{pj,h})}{(T_{hj,i} - T_{cj,i})}, \quad (2)$$

188 where  $c_p$  is the specific heat of fluids.  $m c_p$  as an important variable is referred to as heat  
 189 capacity flow rate of fluids, which can be obtained for the cold and hot fluids in each SHE as  
 190 follows [23]:

$$m_c c_{pj,c} = \frac{q_j}{T_{cj,o} - T_{cj,i}}, \quad (3)$$

$$m_h c_{pj,h} = \frac{q_j}{T_{hj,i} - T_{hj,o}}. \quad (4)$$

191 In view of the one-to-one correspondence between the temperature and specific  
 192 enthalpy at a fixed pressure, the unknown end temperature of each SHE can be obtained  
 193 through the energy balance in each SHE. The energy balance in each SHE can be expressed  
 194 as

$$m_c (h_{cj,o} - h_{cj,i}) = m_h (h_{hj,i} - h_{hj,o}) = q_j. \quad (5)$$

195 Based on the  $\varepsilon - NTU$  method, the local number of heat transfer unit for each counter-  
 196 flow SHE can be written as [24]

$$NTU_j = \frac{\ln((1 - \varepsilon_j)/(1 - R_{cj}\varepsilon_j))}{R_{cj} - 1}, \quad (6)$$

197 where  $R_{cj}$  is defined as

$$R_{cj} = \frac{\min(m_c c_{pj,c}, m_h c_{pj,h})}{\max(m_c c_{pj,c}, m_h c_{pj,h})}. \quad (7)$$

198 For each SHE, the required local heat conductance can be expressed as [24]

$$HA_j = NTU_j \min(m_c c_{pj,c}, m_h c_{pj,h}). \quad (8)$$

199 Summing the local heat conductance yields the required total heat conductance in the  
 200 evaporator:

$$HA = \sum_1^N HA_j. \quad (9)$$

For the check calculation, the total heat conductance is fixed and each SHE has the same local heat conductance. In this circumstance, the local number of heat transfer unit in each SHE can be obtained by

$$Ntu_j = \frac{HA_j}{\min(m_c c_{pj,c}, m_h c_{pj,h})}. \quad (10)$$

The local effectiveness in each SHE can be expressed as

$$\varepsilon_j = \frac{1 - \exp(-NTU_j(R_{cj} - 1))}{1 - R_{cj}\exp(-NTU_j(R_{cj} - 1))}. \quad (11)$$

The affordable local heat load of each SHE can be calculated by

$$q_j = \varepsilon_j \min(m_c c_{pj,c}, m_h c_{pj,h})(T_{hj,i} - T_{cj,i}). \quad (12)$$

The affordable total heat load of the evaporator can be obtained by summing the local heat load. According to the  $\varepsilon - NTU$  method, the unknown end temperatures of cold and hot fluids in each SHE can be obtained by iteration based on the energy balance in Eq. (5).

The entransy dissipation introduced by Guo et al. [21, 25] can be used to reflect the irreversibility of a heat transfer process. The entransy dissipation has been successfully employed to evaluate or optimize heat transfer performance in some recent studies [26-29]. Based on the assumption (c), the local entransy dissipation in each SHE can be expressed as [30-32]

$$\dot{E}_{dis,j} = \frac{1}{2}(m_h c_{pj,h} T_{hj,i}^2 - m_h c_{pj,h} T_{hj,o}^2) + \frac{1}{2}(m_c c_{pj,c} T_{cj,i}^2 - m_c c_{pj,c} T_{cj,o}^2). \quad (13)$$

The total entransy dissipation in the evaporator can be written as

$$\dot{E}_{dis} = \sum_1^N \dot{E}_{dis,j}. \quad (14)$$

Exergy efficiency is another important indicator to the performance of heat exchanger, which reveals the quality of the usable energy transfer [33-35]. Since the working temperature of fluids in the evaporator is below the environmental temperature (assumed to be 293 K), cold exergy is transferred from the cold fluid to the two hot fluids. The total exergy efficiency of the evaporator is defined as

$$\eta_{EX} = \frac{EX_{hl,o} - EX_{hl,i} + EX_{hh,o} - EX_{hh,i}}{EX_{c,i} - EX_{c,o}}. \quad (15)$$

The term  $EX$  represents the flow exergy of each fluid at the respective inlet or outlet in the evaporator, which can be calculated as follows [36, 37]:

$$EX = m[(h - h_0) - T_0(s - s_0)], \quad (16)$$

where  $s$  is the specific entropy of fluid and the subscript 0 denotes the environmental conditions.

By substituting Eq. (16) into Eq. (15), the exergy efficiency can be expressed as

$$\eta_{EX} = \frac{m_{hl}[(h_{hl,o} - h_{hl,i}) - T_0(s_{hl,o} - s_{hl,i})] + m_{hh}[(h_{hh,o} - h_{hh,i}) - T_0(s_{hh,o} - s_{hh,i})]}{m_c[(h_{c,i} - h_{c,o}) - T_0(s_{c,i} - s_{c,o})]}, \quad (17)$$

which combined with the heat balance relation  $m_{hl}(h_{hl,i} - h_{hl,o}) + m_{hh}(h_{hh,i} - h_{hh,o}) = Q_{tot}$  and Eq. (1) yields

$$\eta_{EX} = \frac{T_0[m_{hl}(s_{hl,i} - s_{hl,o}) + m_{hh}(s_{hh,i} - s_{hh,o})] - Q_{tot}}{T_0 m_c(s_{c,o} - s_{c,i}) - Q_{tot}}. \quad (18)$$

### 2.3. Design parameters and calculation procedures

The initial given parameters for both design and check calculations are listed in Table 1. The liquid air is generally stored in a tank at a temperature of about 80 K. When the liquid air is pressurized by a cryogenic pump for flowing into the evaporator to release cold energy, its temperature is generally increased to about 83 K [9, 10]. Thus, the inlet temperature of cold

fluid is set to 83 K. The inlet pressure of cold fluid is set to 5 MPa, 7 MPa and 9 MPa to explore its effects on heat exchange performance of the evaporator. The inlet pressures of hot fluids are set to atmospheric pressure, i.e. 0.1 MPa. As mentioned in Section 2.1, propane and methanol are selected as hot fluids to successively heat up the cold fluid N<sub>2</sub>. The temperature-dependent specific enthalpies and entropies of N<sub>2</sub>, propane and methanol at prescribed pressures were extracted from NIST standard database [38]. The temperature-dependent specific enthalpies are also depicted in Fig. 3. Based on the assumption (e), it is confirmed that these isobaric specific enthalpies can be used to support the calculations for the whole evaporator at a specified inlet pressure. Fig. 3(a) shows that the specific enthalpy of N<sub>2</sub> at a fixed pressure varies nonlinearly with the temperature. According to the freezing points and boiling points of the hot fluids at the pressure of 0.1 MPa as shown in Fig. 3(b) combined with the assumption (g), it can be deduced that the operating temperature of propane and methanol should be maintained between 90.5 K and 225.7 K and between 180.6 K and 332.3 K, respectively. In light of the assumption (f), it can be further obtained that the inlet temperature of propane or the outlet temperature of methanol should be maintained between 180.6 K and 225.7 K for reliable operation, as shown in Fig. 3(b).

Table 1 The initial given data for design and check calculation.

Parameters	Values for design calculation	Values for check calculation
Inlet pressure of cold fluid, $P_c$ (MPa)	5, 7, 9	5, 7, 9
Inlet temperature of cold fluid, $T_{c,i}$ (K)	83	83
Outlet temperature of hot fluid, $T_{c,o}$ (K)	283	-
Heat conductance, HA (MW/K)	-	4
Mass flow rate of cold fluid, $m_c$ (kg/s)	100	100
Inlet pressure of hot fluids, $P_h$ (MPa)	0.1	0.1
Inlet temperature of hot fluid at high temperature section, $T_{hh,i}$ (K)	288	288
Outlet temperature of hot fluid at low temperature section, $T_{hl,o}$ (K)	93	93
Number of SHEs, $N$	80	80

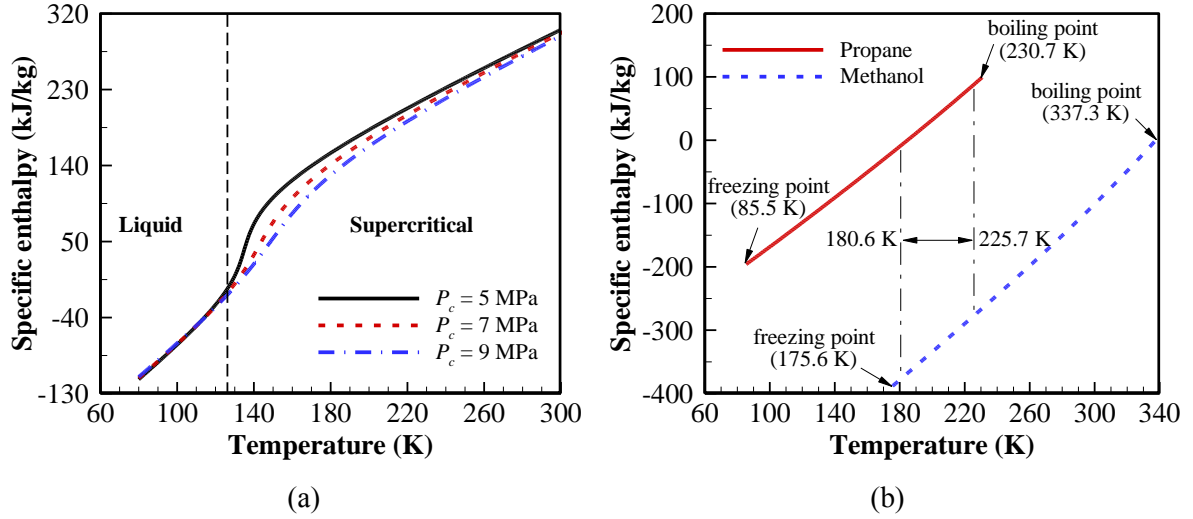


Fig. 3. The temperature-dependent specific enthalpies at specified pressures: (a)  $N_2$  at  $P_c=5$  MPa,  $P_c=7$  MPa, and  $P_c=9$  MPa; and (b) propane and methanol at  $P_h=0.1$  MPa.

Fig. 4(a) illustrates the calculation procedures for design calculation, which includes the input and output parameters. The input parameters,  $m_{hh}$  and  $\tau$ , are not the initial design parameters and thus not specified in Table 1. They are variable and need to be given and adjusted to reveal their effects on heat exchange performance. The critical parameter  $m_{hl}$  is initially supposed to start the iterations. Subsequently, the local parameters are successively calculated for each SHE starting from the outlet of cold fluid, except for the first SHE. The  $m_{hl}$  is then refreshed based on the first SHE using Eq. (5) for the next iteration until satisfying convergence criterion. In the new iterations after the  $m_{hl}$  is refreshed, the calculations of local parameters for the high temperature section can be skipped. After the calculation convergence is achieved, some local or holistic parameters can be easily obtained, including mass flow rate and inlet temperature of hot fluid in the low temperature section, effectiveness, entransy dissipation and required heat conductance.

Fig. 4(b) depicts the calculation procedures for check calculation, which involves one more iteration loop compared to the procedures for design calculation. Similarly, the input parameters,  $m_{hl}$  and  $\varphi$ , are variable and need to be given and adjusted to reveal their effects

on heat exchange performance. In the iteration loop of inner layer, the supposed parameter  $q_j$  for each SHE is repeatedly refreshed until convergence. In the iteration loop of middle layer, the calculation of local parameters for each SHE, except for the last SHE, starts from the inlet of cold fluid, since the outlet temperature of cold fluid is unknown. In the iteration loop of outer layer, the supposed parameter  $m_{hh}$  is repeatedly refreshed based on the last SHE until convergence. Similarly, in the new iterations after the  $m_{hh}$  is refreshed, the calculations of local parameters for the low temperature section can be skipped. After the calculation convergence is achieved, some local or holistic parameters can be easily obtained, including mass flow rate of hot fluid in the high temperature section, inlet temperature of hot fluid in the low temperature section, effectiveness, entransy dissipation and affordable heat load.

For simulating the heat exchange characteristics of the T-N<sub>2</sub> evaporator, two sets of programs were developed in the MATLAB software based on the above calculation procedures for the design and check calculations, respectively.



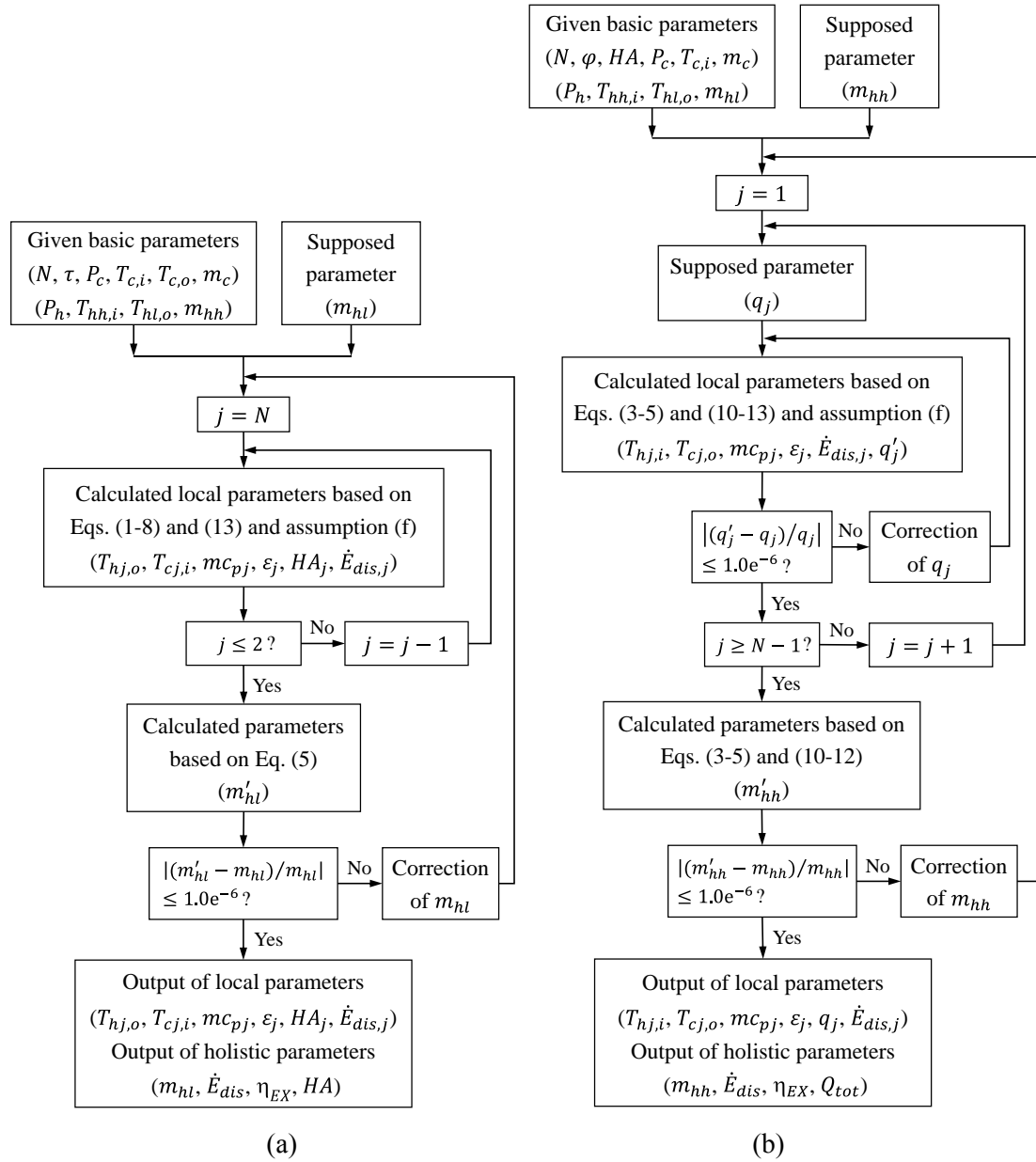


Fig. 4 Calculation procedures for (a) design calculation (b) check calculation.

#### 2.4. Segment independent study

The number of SHEs ( $N = 80$ ) as listed in Table 1 is determined by segment independent test. Four different numbers of SHEs, 20, 40, 80 and 160, were used to obtain a segment independent solution. For the segment independent test of design calculation, the heat load ratio of low temperature section was set to 65% and the mass flow of methanol was set to 60 kg/s. The predicted total entransy dissipation and total heat conductance for design

calculation with the four segment settings are shown in Table 2. Similarly, for the segment independent test of check calculation, the heat conductance ratio of low temperature section was set to 65% and the mass flow of propane was set to 120 kg/s. The predicted total entransy dissipation and mass flow of methanol for check calculation with the four segment settings are shown in Table 2. The relative difference between values predicted with two adjacent segment settings is denoted by  $D_{re}$ , which is also listed in Table 2. From the table, it is obvious that all the relative differences of the selected four parameters are less than 0.05% between the segment settings of  $N = 80$  and  $N = 160$ . Therefore, the segment setting of  $N = 80$  is selected for both design and check calculations to complete the numerical predictions in the following section.

Table 2 Segment independent results for design and check calculations.

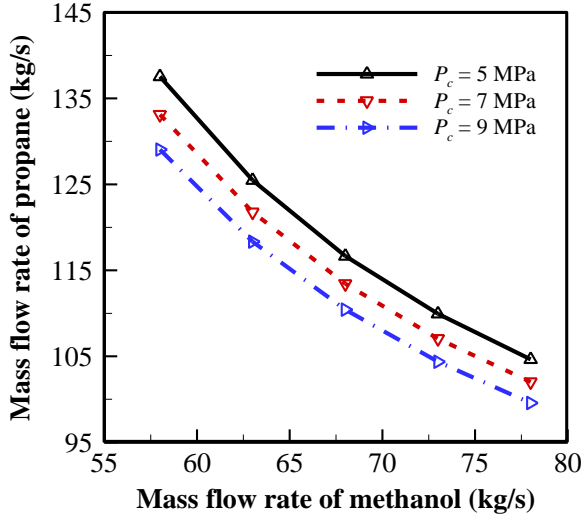
$N$	Design calculation				Check calculation			
	$\dot{E}_{dis}(\text{MW}\cdot\text{K})$	$D_{re}(\%)$	$HA(\text{MW/K})$	$D_{re}(\%)$	$\dot{E}_{dis}(\text{MW}\cdot\text{K})$	$D_{re}(\%)$	$m_{hh}(\text{kg/s})$	$D_{re}(\%)$
20	384.53	-	4.2923	-	428.46	-	55.5819	-
40	385.64	0.29	4.2947	0.06	431.07	0.61	55.4567	0.23
80	385.92	0.07	4.2953	0.01	431.79	0.17	55.4218	0.06
160	385.98	0.02	4.2955	0.00	431.97	0.04	55.4119	0.02

### 3. Results and discussions

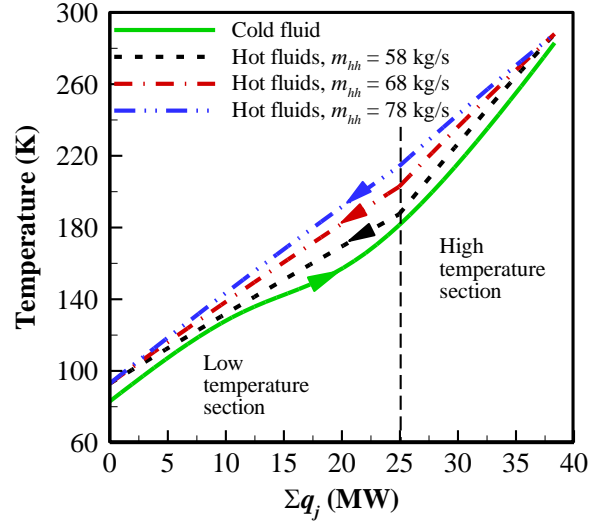
#### 3.1. Design calculation

As listed in Table 1, the inlet and outlet temperatures of cold fluid as well as its mass flow rate are fixed, and thus the total heat load and local heat transfer rate are fixed. The inlet temperature of hot fluid at the high temperature section and outlet temperature of hot fluid at the low temperature section are also fixed to determine the mass flow rate of propane, under the selected mass flow rate of methanol and the selected heat load ratio of low temperature section based on the assumption (f). The heat load ratio of low temperature section was set to 65% as an illustration. The quantitative relations of the mass flow rates of the two hot fluids

under different pressures of cold fluid are shown in Fig. 5(a). The mass flow rate of propane decreases with the increase in that of methanol. Since the corresponding relation is unique at a specified pressure of cold fluid, only the mass flow rate of methanol  $m_{hh}$  is referred to in the following for convenience. Fig. 5(b) illustrates the relations of temperature with the local heat transfer rate accumulation under different mass flow rates of hot fluids. The temperature shows twisty variation along the flow direction of cold fluid in spite of same local heat transfer rate existing in each SHE, which is attributed to the varying specific heat of  $N_2$ . With the decrease in  $m_{hh}$ , the pinch point in the low temperature section gradually moves from the inlet of cold fluid to the interior for the whole evaporator and the temperature difference at the pinch point also gradually decreases as indicated in Fig. 5(b). This implies that the violently varying properties of fluids easily result in the temperature cross or violating the pinch constraints, which makes the evaporator invalid. The calculation indicates that when  $m_{hh} \leq 55$  kg/s the temperature cross will occur. Therefore, it is of vital importance to carefully tailor the relevant parameters in the design of T- $N_2$  heat exchanger. In addition, Fig. 5 (b) indicates that the required inlet temperature of hot fluid in the low temperature section descends with the decreases in  $m_{hh}$ .



(a)



(b)

Fig. 5. The relations of (a) mass flow rates of the two hot fluids under different pressures of cold fluid at  $\tau = 65\%$ , and (b) temperature with local heat transfer rate accumulation in SHEs at  $P_c = 7$  MPa and  $\tau = 65\%$ .

Fig. 6(a) shows the relations of local heat capacity flow rate with the local heat transfer rate accumulation under different mass flow rates of hot fluids. Along the flow direction of cold fluid, the heat capacity flow rate of cold fluid first increases and then decrease while the heat capacity flow rates of hot fluids gradually increase in both the two sections. The inflection point of changing trend for the heat capacity flow rate of cold fluid exists at the low temperature section. The changing range of heat capacity flow rate of cold fluid is much larger than those of hot fluids. The discrepancy of the heat capacity flow rates between hot fluids in the two sections decreases with the increase in  $m_{hh}$ . The variation curves of the heat capacity flow rates of cold and hot fluids intersect with each other at some locations, and the number of intersection points reduces from 3 to 1 when  $m_{hh}$  increases from 58 kg/s to 78 kg/s. The local heat capacity rate ratio is defined as

$$R_{cj,hc} = \frac{m_h c_{pj,h}}{m_c c_{pj,c}}. \quad (19)$$

Obviously, the local heat capacity rate ratio equals one at these intersection points as shown in Fig. 6(a). The respective average heat capacity flow rates of cold and hot fluids in the two temperature sections are summarized in Fig. 6(b) in the form of column. It can be found that the average heat capacity flow rates of hot fluids in both the two sections are closer to those of cold fluid as  $\dot{m}_{hh}$  decreases. The more the number of intersection points is, the closer the average heat capacity flow rates of the hot fluids are to that of cold fluid. The relationship between the local heat capacity flow rates of hot and cold fluids is closely related to the local performance, while the relationship between the average heat capacity flow rates is closely related to the total performance.

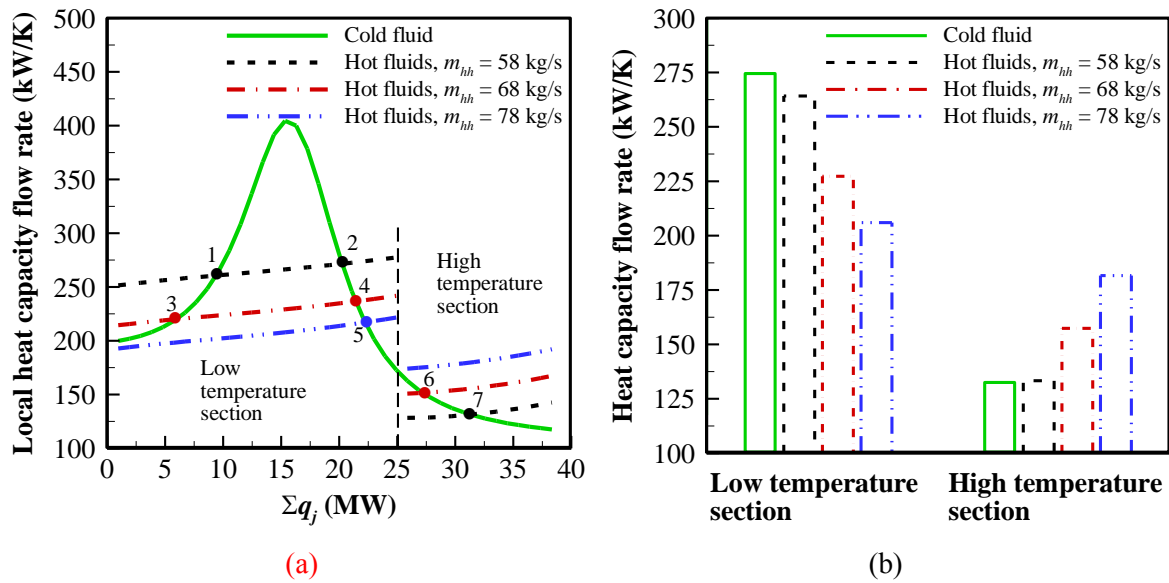


Fig. 6. (a) The variation of local heat capacity flow rate with local heat transfer rate accumulation in SHEs and (b) average heat capacity flow rate for cold and hot fluids at  $P_c = 7$  MPa and  $\tau = 65\%$ . The intersection points are marked with dots and numbers.

The variations of local logarithmic mean temperature difference and local heat conductance in the SHEs along the flow direction of cold fluid are elucidated in Fig. 7. The local logarithmic mean temperature difference for each counter-flow SHE is defined as

$$\Delta T_m = \frac{(T_{hj,o} - T_{cj,i}) - (T_{hj,i} - T_{cj,o})}{\ln((T_{hj,o} - T_{cj,i})/(T_{hj,i} - T_{cj,o}))} \quad (20)$$

Due to the fixed local heat transfer rate in each SHE, the local mean temperature difference shows varying trends opposite to local heat conductance as shown in Fig. 7. The local mean temperature difference and local heat conductance non-monotonically along the flow direction of cold fluid in both the two temperature sections in the cases of smaller  $m_{hh}$ . The position of the minimum local mean temperature difference or the required maximum local heat conductance in the low temperature section moves toward the flow direction of cold fluid as  $m_{hh}$  decreases. With the decrease in  $m_{hh}$ , the local mean temperature difference in each SHE generally decreases, and accordingly the local heat conductance required by each SHE increases in both the two temperature sections, whilst the heat conductance required by the whole low temperature section exhibits larger increment than that required by the whole high temperature section.

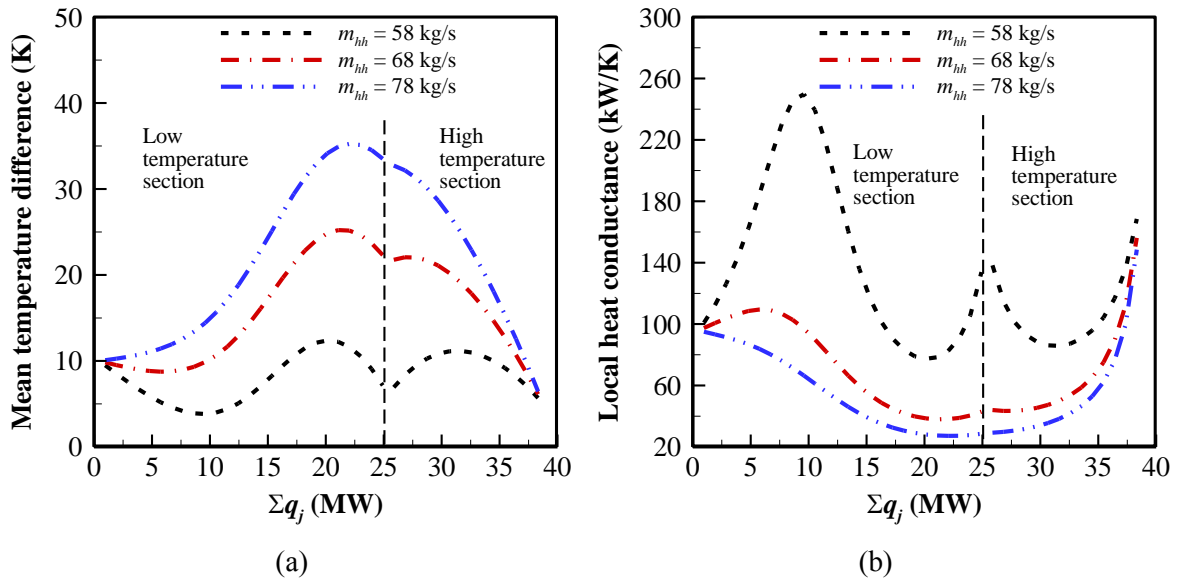


Fig. 7. The variations of (a) local logarithmic mean temperature difference and (b) local heat conductance with heat transfer rate accumulation in SHEs at  $P_c = 7$  MPa and  $\tau = 65\%$ .

Fig. 8 depicts the local effectiveness and local entransy dissipation in SHEs along the flow direction of cold fluid under different mass flow rates of hot fluids. According to the variations of the two local parameters, it can be found that the fall of  $m_{hh}$  generally improves the performance of each SHE under the same other conditions. The performance gap between different mass flow rates of hot fluids in the high temperature section decreases along the flow direction of cold fluid, while that in the low temperature section presents the varying trend similar to “N” shape as shown in Fig. 8(a). Comparing Figs. 8(b) and 7(a), we can find that the local entransy dissipation has very similar changing trend with the local mean temperature difference. This is because the irreversibility of heat transfer is primarily caused by the temperature difference when heat leak and flow friction loss is negligible. By comparing Fig. 8 with Fig. 6(a), the maximum local effectiveness and the minimum local entransy dissipation appear around the positions of  $R_{cj,hc} = 1$ , when the heat capacity flow rates of cold and hot fluids have the same changing tendency along the flow direction of cold fluids. On the contrary, if the two heat capacity flow rates have the opposite changing tendencies, around the positions of  $R_{cj,hc} = 1$  exist the minimum local effectiveness and the maximum local entransy dissipation. Therefore, the same changing tendency of the heat capacity flow rates of two sides in the SHEs is beneficial for the improvement of local heat exchange performance.

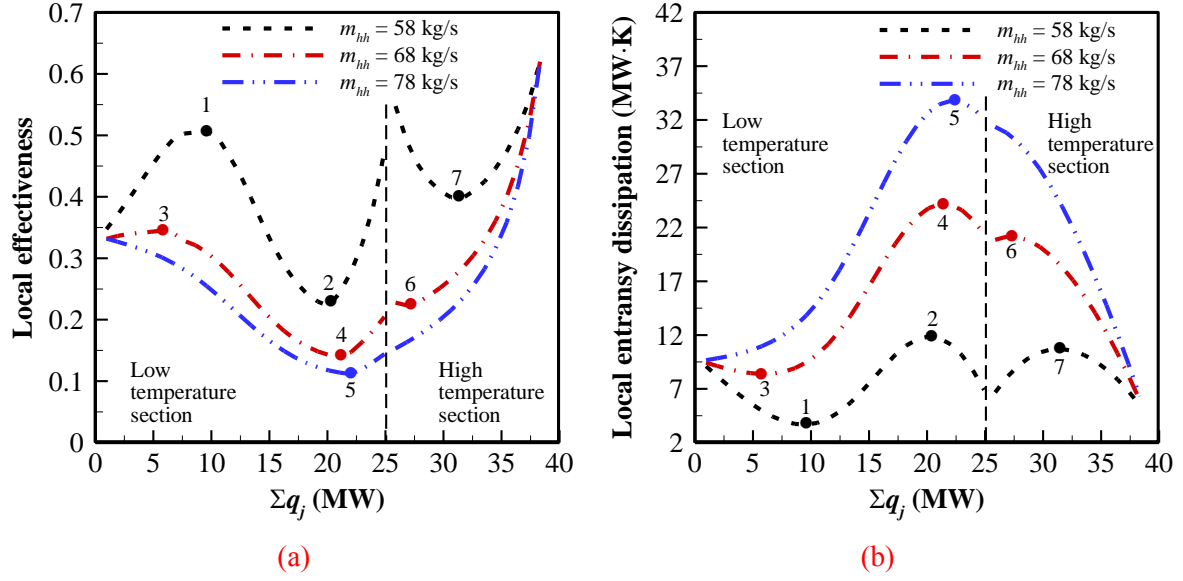
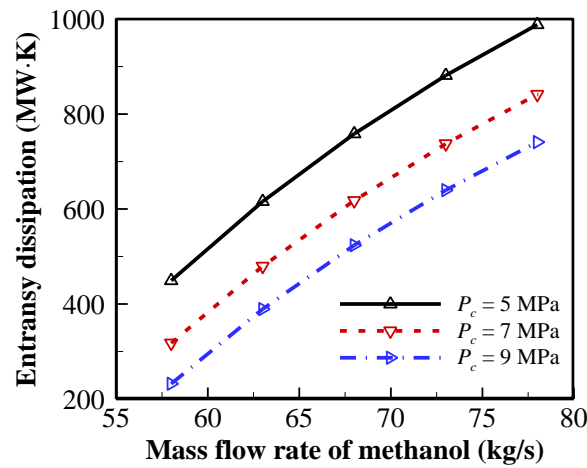


Fig. 8. The variations of (a) local effectiveness and (b) local entransy dissipation with heat transfer rate accumulation in SHEs at  $P_c = 7$  MPa and  $\tau = 65\%$ . The locations of extremums are marked with dots and numbers.

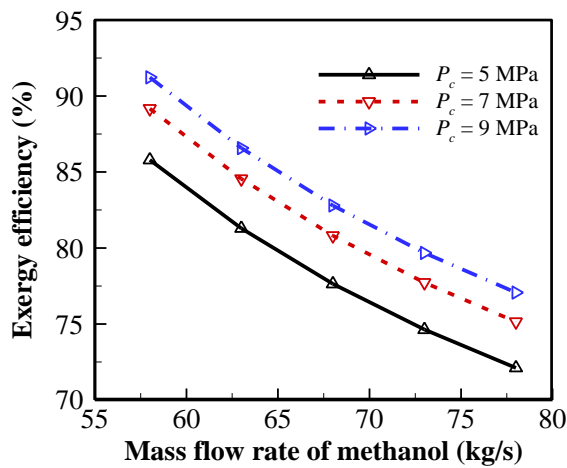
To evaluate the overall performance of T-N<sub>2</sub> evaporator, the variations of the total entransy dissipation and exergy efficiency with  $m_{hh}$  under different pressures of cold fluid are demonstrated in Figs. 9(a) and 9(b), respectively. The total entransy dissipation decreases as the pressure of cold fluid increases at the same mass flow rate and decreases with the decrease in  $m_{hh}$  at the same pressure, while the exergy efficiency shows totally opposite change trends. In combination with Fig. 6(b), it can be inferred that making the average heat capacity flow rate of hot fluids closer to that of cold fluid is beneficial to improving the heat exchange performance of the evaporator. By comparing Figs. 9(a, b) and 5(b), it is obvious that the smaller the temperature difference between hot and cold fluids at the junction of the two temperature section, the better the heat exchange performance of the evaporator. The calculation indicates that the extractable cold amount from the liquid N<sub>2</sub> with the same temperature rise from 83 K to 283 K decreases with the increase in the pressure of N<sub>2</sub>, which is caused by the decrease of its specific enthalpy as shown in Fig. 3(a). Specially, the extractable cold amount from unit mass of liquid N<sub>2</sub> decreases from 389.01 kJ/kg to 377.74



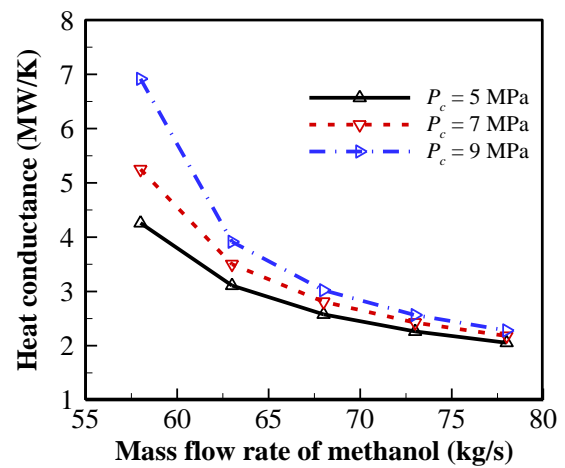
kJ/kg when the pressure increases from 5 MPa to 9 MPa. The manufacture cost of heat exchanger is mainly determined by the heat conductance. Fig. 9(c) shows the variations of required total heat conductance with  $m_{hh}$  under different pressures of cold fluid. It is clear that the total heat conductance shows the varying tendencies opposite to the total entransy dissipation number. This indicates that the improvement of the whole performance of evaporator is at the expense of requiring larger area or/and coefficient of heat transfer. In addition, the effect of the pressure of cold fluid on the required total heat conductance gradually diminishes with the increase in  $m_{hh}$ .



(a)



(b)



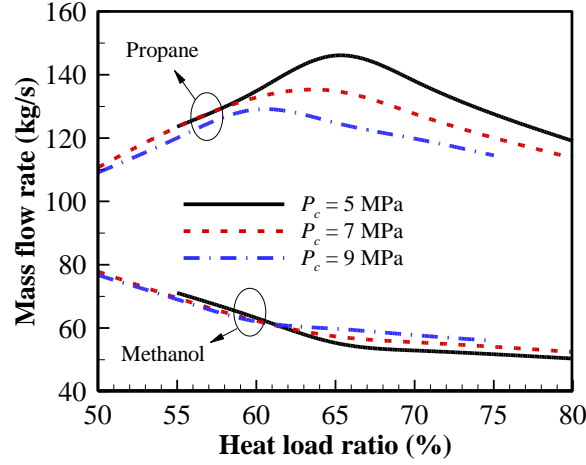
(c)

Fig. 9. The variations of (a) total entransy dissipation, (b) total exergy efficiency and (c) required total heat conductance with mass flow rate of methanol under different pressures of cold fluid at  $\tau = 65\%$ .

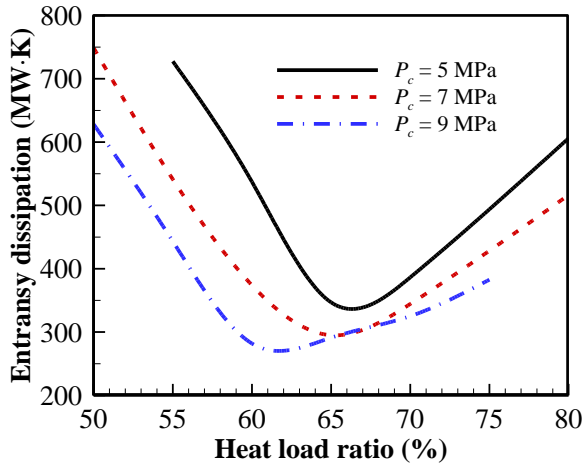
442

443         In the above study, the heat load distribution ratio between the two temperature sections  
444 is selectively fixed. However, it is very pivotal for the performance of the evaporator and thus  
445 need to be elaborately considered in the design calculation. In order to compare heat  
446 exchange features under different heat load distribution ratios, the temperature difference  
447 between the hot and cold fluids at the junction of the two temperature section was kept 5 K. If  
448 this constraint condition cannot be satisfied at some heat load distribution ratios due to the  
449 assumption (g), the temperature of the hot fluids at the junction of the two-temperature  
450 section were fixed at 180.6 K, which is the lowest reliable operating temperature at the  
451 junction as mentioned in Section 2.3. Therefore, the minimum temperature difference  
452 between hot and cold fluids at the junction of the two temperature sections is achieved under  
453 the constraint of the assumption (g). The above conditions can be satisfied by adjusting the  
454 mass flow rates of propane and methanol. Based on the known data in Table 1, the mass flow  
455 rates of propane and methanol, the entransy dissipation and the exergy efficiency at different  
456 heat load ratios of the low temperature section among the whole evaporator are illustrated in  
457 Fig. 10. It can be found from Fig. 10(a) that the required mass flow rate of propane first  
458 increases and then decreases with the increase in the heat load ratio of the low temperature  
459 section, while that of methanol gradually decreases. Fig. 10(b) indicates that the minimum  
460 entransy dissipation can be achieved by adjusting heat load ratio of the low temperature  
461 section and it decreases with the increase in  $P_c$ . The heat load ratios of the low temperature  
462 section corresponding to the minimum values of entransy dissipation at  $P_c = 5$  MPa,  $P_c = 7$   
463 MPa and  $P_c = 9$  MPa are about 66%, 65% and 61%, respectively, which also correspond to  
464 the respective maximum mass flow rate of propane as shown in Fig. 10(a). By comparing  
465 Figs. 10(c) and 10 (b), it can be found that the exergy efficiency achieves the maximum as  
466 the entransy dissipation achieves the minimum under various pressures of cold fluids. It

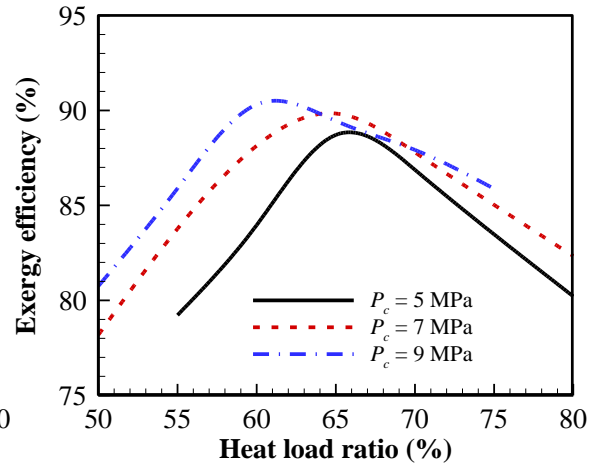
manifests that the exergy efficiency and the entransy dissipation are congenerous in performance evaluation of the evaporator when the heat load is fixed.



(a)



(b)



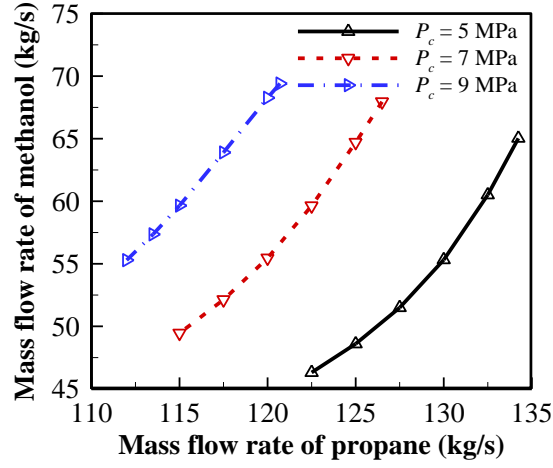
(c)

Fig. 10. The effects of heat load ratio of low temperature section on (a) the required mass flow rates of propane and methanol, (b) the entransy dissipation and (c) the exergy efficiency.

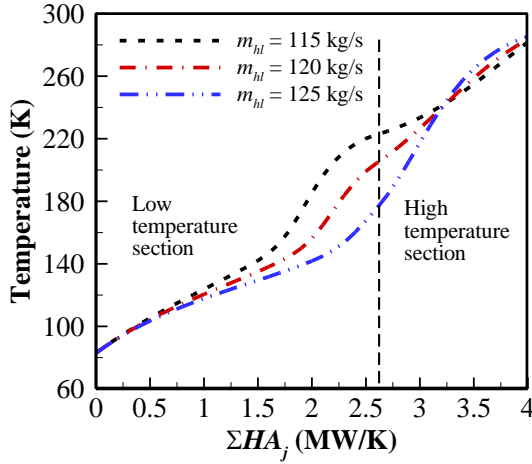
### 3.2. Check calculation

In this subsection, the total heat conductance of T-N<sub>2</sub> evaporator is given to analyze its heat exchange performance and examine its affordable heat load. As listed in Table 1, the total heat conductance is specified as  $4 \times 10^6$  W/K. The heat conductance ratio of the low temperature section is set to 65% as an illustration. Similar to Fig. 5(a), the mass flow rate of

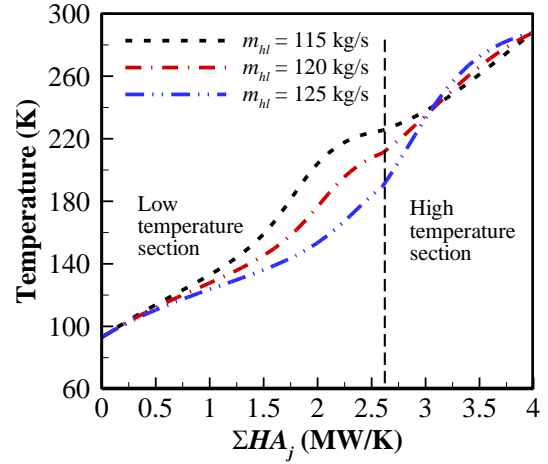
methanol is also determined by that of propane because of a temperature equality of two hot fluids at the junction of the two temperature sections in the assumption (f). The relations of the mass flow rates of the two hot fluids under different pressures of cold fluid are shown in Fig. 11(a). The required mass flow rate of methanol increases with that of propane under the given parameters of check calculation in Table 1. In order to ensure that the hot fluids stay liquid and avoid the invalidation of evaporator, the valid ranges of the mass flow rate of propane are different at different cold fluid pressures. For convenience of description, the mass flow rate of propane  $m_{hl}$  is used to indicate the variation of the mass flow rates of hot fluids in the following. Figs. 11(b) and 11(c) depict the temperature profiles of cold and hot fluids along the flow direction of cold fluid at different  $m_{hl}$ , respectively. The cold and hot fluids exhibit similar temperature profiles at the same  $m_{hl}$ . The temperature rise of cold fluid in the low temperature section diminishes with the increase in  $m_{hl}$ , which requires lower inlet temperature of propane; whereas the change is inverse in the high temperature section, which requires larger mass flow rate of methanol. Therefore, the eventual outlet temperature of cold fluid still increases with  $m_{hl}$ .



(a)



(b)



(c)

Fig. 11. (a) The relations of mass flow rates of the two hot fluids under different pressures of cold fluid at  $\varphi = 65\%$ , and the temperature variations of (b) cold and (c) hot fluids with local heat conductance accumulation in SHEs at  $P_c = 7$  MPa and  $\varphi = 65\%$ .

Fig. 12 elucidates the variations of local heat capacity rate ratio and local heat transfer rate in the SHEs along the flow direction of cold fluid. Obviously, the local heat capacity rate ratio first decreases and then increases along the flow direction of cold fluid in the low temperature section, while it increases all along in the high temperature section as shown in Fig. 12(a). The local heat capacity rate ratio also shows non-monotonic variation with the increase in  $m_{hl}$ . This is because the fluids work at markedly different temperature regions at different  $m_{hl}$  as shown in Fig. 11(b), which makes the fluids have notably different specific heat as depicted in Fig. 1. As shown in Fig. 12(b), the gap of the local heat transfer rate

among different SHEs at the same  $m_{hl}$  increases with the decrease in  $m_{hl}$  in the low temperature section, while the situation is inverse in the high temperature section. The maximum gap at  $m_{hl} = 115$  kg/s is up to eightfold. Fig. 12(b) also indicates that there exist extremums of the local heat transfer rates in both the two sections, whose position and number are corresponding to those of  $R_{cj,hc} = 1$  as shown in Fig 12(a). The changing tendency of the local heat transfer rate exhibits reversals twice along the flow direction of cold fluid at different positions of  $R_{cj,hc} = 1$  in the low temperature section. Hence, the variation of local heat transfer rate highly dependent on the heat capacity rate ratio.

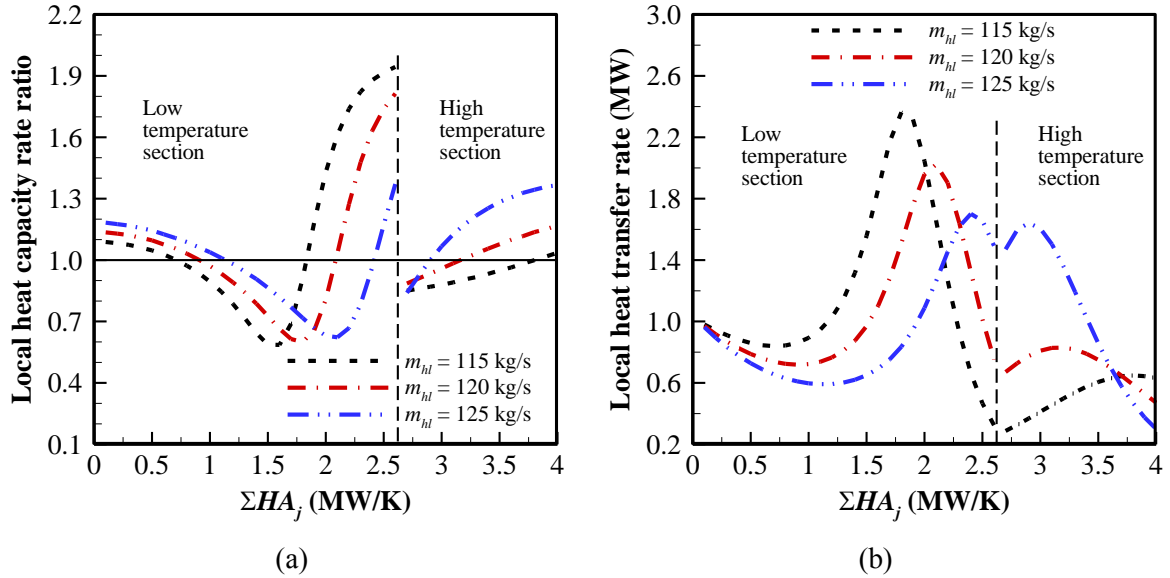


Fig. 12. The variations of (a) local heat capacity rate ratio and (b) local heat transfer rate with heat conductance accumulation in SHEs at  $P_c=7$  MPa and  $\varphi = 65\%$ .

The variations of the local effectiveness in the SHEs along the flow direction of cold fluid are illustrated in Fig. 13(a). In the low temperature section, the local effectiveness along the flow direction of cold fluid decreases before the first position of  $R_{cj,hc} = 1$  and sharply increases after the second position of  $R_{cj,hc} = 1$ , while it keeps nearly constant between the two positions; the local effectiveness tends to be constant with the increase in  $\dot{m}_{hl}$  before the

first position of  $R_{cj,hc} = 1$ , whilst it basically decreases after the first position of  $R_{cj,hc} = 1$ . In the high temperature section, the local effectiveness decreases before  $R_{cj,hc} = 1$  and increases after  $R_{cj,hc} = 1$ ; the local effectiveness has no explicit changing tendency with the increase in  $m_{hl}$ . Fig. 13(b) shows the variations of the local entransy dissipation with heat conductance accumulation in the SHEs. Along the flow direction of cold fluid, the local entransy dissipation shows changing trends basically similar to the local heat transfer as shown in Fig. 12(b). The larger the local heat transfer rate, the stronger the irreversibility of heat transfer. At smaller  $m_{hl}$ , the variation amplitude of local entransy dissipation in the low temperature section is notably larger than that in the high temperature section. As  $m_{hl}$  increases, the maximum local entransy dissipation decreases in the low temperature section, while it increases in the high temperature section. This implies that the entransy dissipation shift from the low temperature section to the high temperature section as  $m_{hl}$  increases. The positions of maximum local entransy dissipation in the two temperature sections both move towards the junction of the two temperature sections with the increase in  $m_{hl}$ .

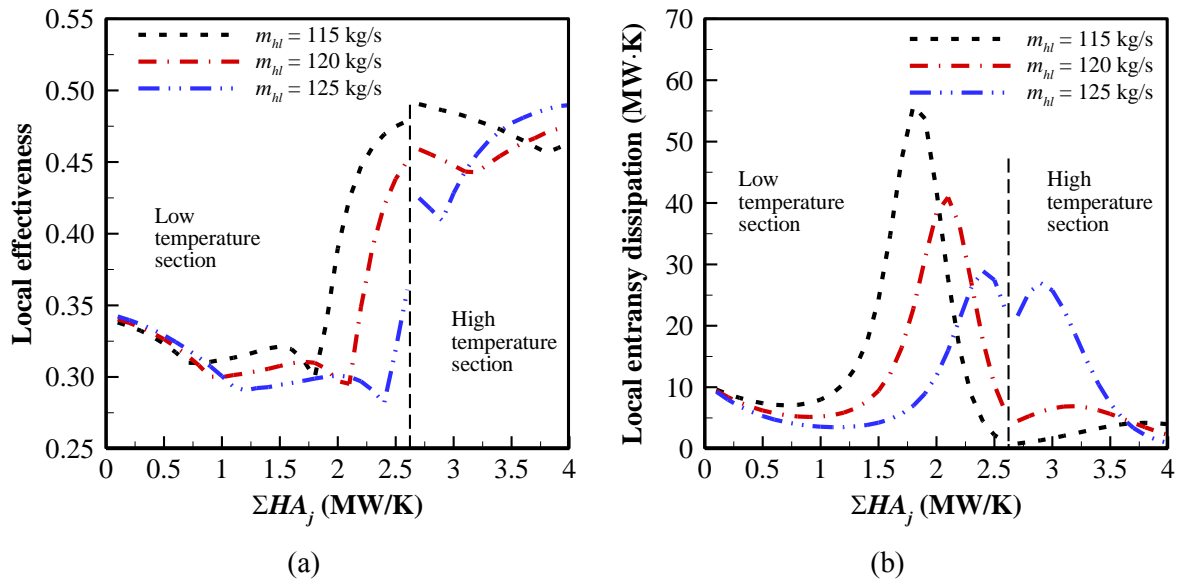
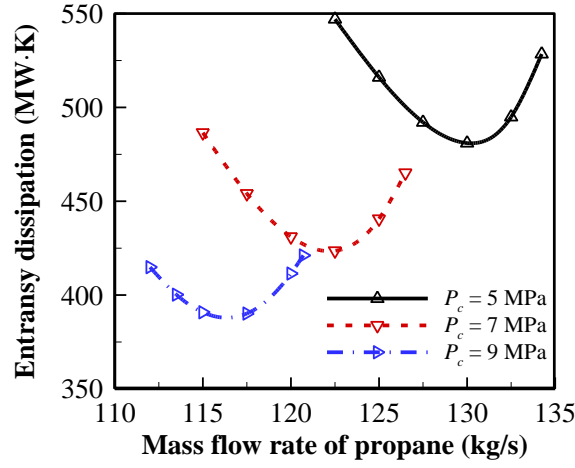


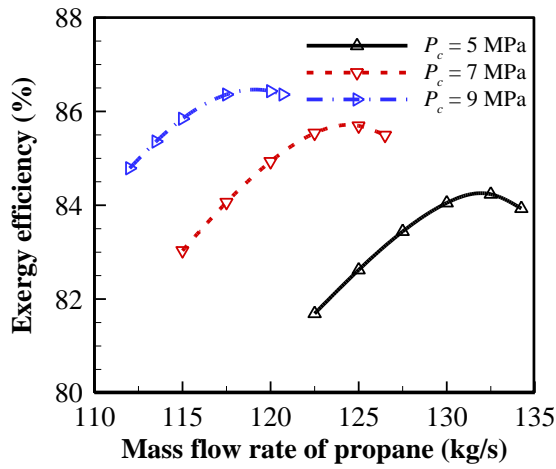
Fig. 13. The variations of (a) local effectiveness and (b) local entransy dissipation with heat conductance accumulation in SHEs at  $P_c=7$  MPa and  $\varphi = 65\%$ .

Fig. 14 displays the variations of total entransy dissipation, total exergy efficiency and affordable total heat load of the evaporator with  $m_{hl}$ . As shown in Figs. 14(a) and 14(b), there exist the minimum total entransy dissipation and the maximum total exergy efficiency at each given pressure of cold fluid and the corresponding  $m_{hl}$  decreases with the increase in the pressure of cold fluid. However, the  $m_{hl}$  corresponding to the maximum exergy efficiency is higher than that corresponding to the minimum entransy dissipation. Therefore, the exergy efficiency and the entransy dissipation cannot be considered the same indicator to the performance of the evaporator. As the pressure of cold fluid increases, the minimum entransy dissipation decreases and the maximum exergy efficiency increases. This manifests that a high cold fluid pressure is favourable for improving the heat exchange performance of evaporator and the optimum heat exchange performance can be achieved by adjusting the mass flow rates of the hot fluids. From Fig. 14(c), it can be seen that the affordable total heat load increases as  $m_{hl}$  increases in their respective valid ranges and decreases as the pressure of cold fluid increases. This implies that increasing the cold fluid pressure will leads to the diminution of the extractable cold amount from the liquid  $N_2$  through the T- $N_2$  evaporator with a given total heat conductance.

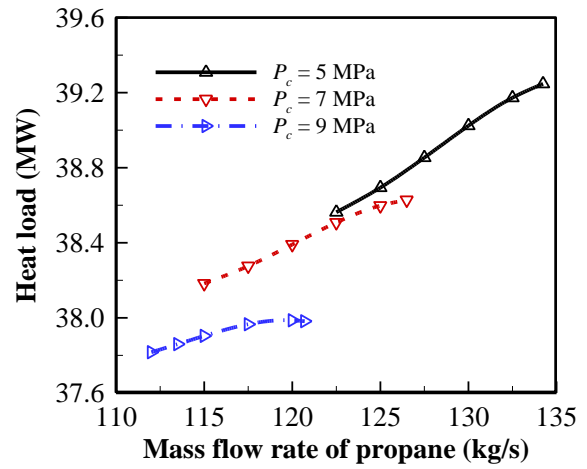




(a)



(b)



(c)

Fig. 14. The variations of (a) total entransy dissipation, (b) total exergy efficiency and (c) affordable total heat load with mass flow rate of propane under different pressures of cold fluid at  $\varphi = 65\%$ .

Similarly, the heat conductance distribution ratio between the two temperature sections is critical for the performance of the evaporator, which thus needs to be detailedly explored in the check calculation. The mass flow rates of the hot fluids were adjusted to obtain the respective minimum entransy dissipation and maximum exergy efficiency at various heat conductance distribution ratios for comparison. Fig. 15(a) depicts the variations of the minimum entransy dissipation and the corresponding outlet temperature of  $N_2$  with the heat conductance ratio of the low temperature section. Among the various ratios, the minimum entransy dissipation is the smallest at the ratio of about 77%, which slightly changes with the pressure of  $N_2$ . The outlet temperatures of  $N_2$  at the various pressures very close to each other

and decrease with the increase in the ratio. This means that heat exchange capacity diminishes with the increase in the ratio when keeping the respective minimum entransy dissipation. The outlet temperature of  $N_2$  is about 274 K at the ratio of 77%. Provided that the required outlet temperature is 283 K, the heat exchange capacity is insufficient when the ratio is set to 77%, although the entransy dissipation is the smallest under the circumstance. Simultaneously considering the demands for the outlet temperature of 283 K and smaller entransy dissipation, the heat conductance ratio of the low temperature section should be set as about 67% for various pressures of  $N_2$ . The required mass flow rates of propane and methanol corresponding to the minimum entransy dissipation at different heat conductance ratios of the low temperature section are illustrated in Fig. 15(b). It can be found that the required mass flow rate of propane increases with the increase in the heat conductance ratio of the low temperature section, while that of methanol gradually decreases. Fig. 15(c) summarized the maximum exergy efficiency and the corresponding outlet temperature of  $N_2$  under various heat conductance ratios of the low temperature section. The maximum exergy efficiency progressively increases with the ratio and keeps nearly constant when the ratio is more than 80%, while the outlet temperatures of  $N_2$  decrease with the increase in the ratio. Simultaneously considering the demands for the outlet temperature of 283 K and larger exergy efficiency, the heat conductance ratio of the low temperature section should be set as about 69% for various pressures of  $N_2$ . The required mass flow rates of propane and methanol corresponding to the maximum exergy efficiency at various heat conductance ratios of the low temperature section are illustrated in Fig. 15(d). In comparison with Fig. 15(b), it can be seen that the required mass flow rates of propane and methanol to achieve the maximum exergy efficiency are both larger than those to achieve the minimum entransy dissipation. The above results indicate that the exergy efficiency and the entransy dissipation are not congenerous in performance evaluation of the evaporator when the heat conductance is fixed,

and therefore a compromise need to be made between the maximum exergy efficiency and the minimum entransy dissipation.

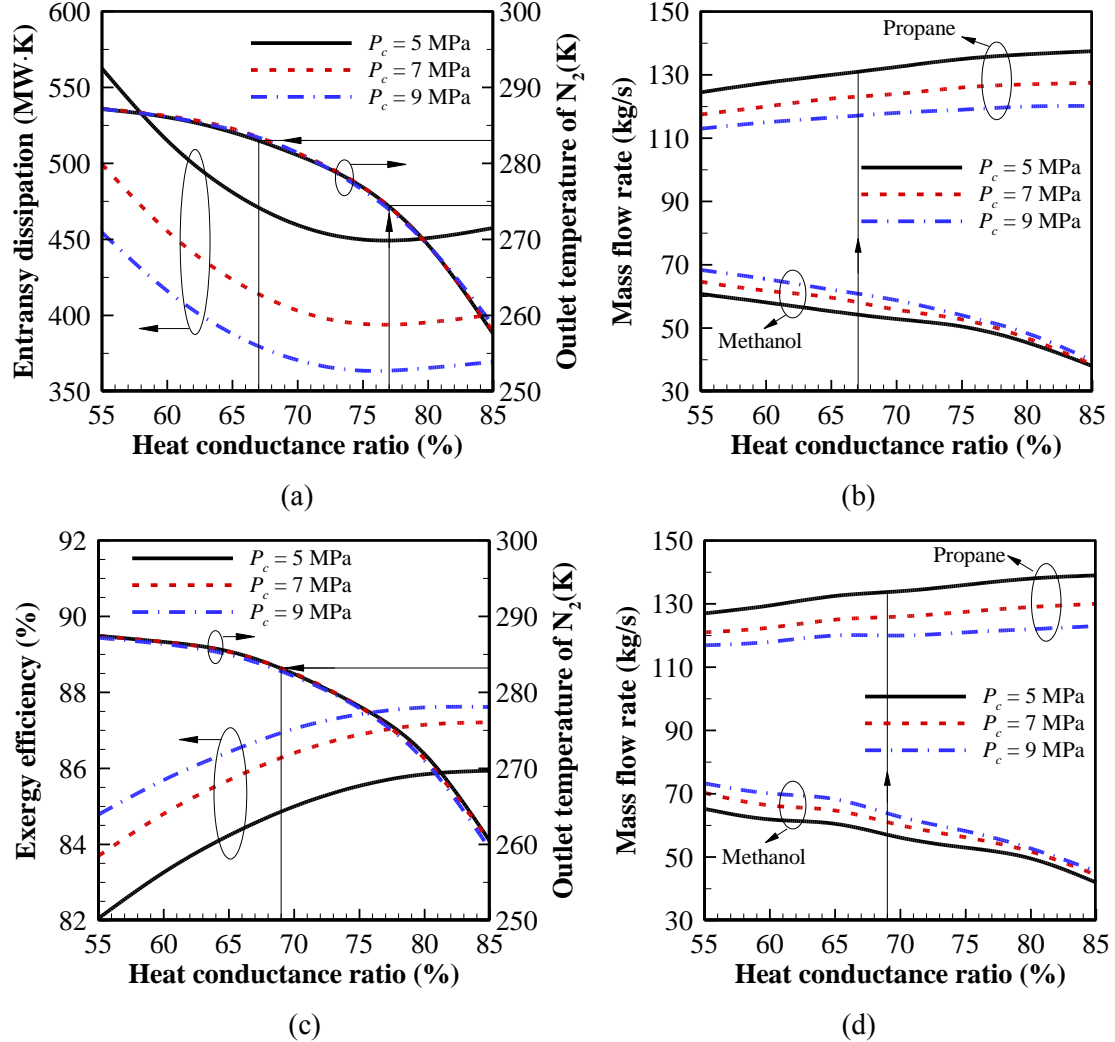


Fig. 15. The effects of heat conductance ratio of low temperature section: (a, b) minimum entransy dissipation, corresponding outlet temperature of  $N_2$  and corresponding mass flow rates of propane and methanol; (c, d) maximum exergy efficiency, corresponding outlet temperature of  $N_2$  and corresponding mass flow rates of propane and methanol.

#### 4. Conclusions

The heat exchange performance analysis of T- $N_2$  evaporator used for cold storage or recovery in the LAES system is implemented in this paper. Due to violent variation of

specific heat of  $N_2$  in the evaporator, the segmental design method is applied. The evaporator is divided into a low temperature section and a high temperature section according to two types of hot fluids (propane and methanol) used to receive the cold energy from the cold fluid  $N_2$ .

When the total heat load is fixed, the local effectiveness and local heat conductance exhibit change trends opposite to local entransy dissipation along the flow direction of  $N_2$ . The local entransy dissipation achieves the minimum around the positions where the local heat capacity rate ratio equals one when the heat capacity flow rates of cold and hot fluids exhibit the same change trend along the flow direction of  $N_2$ , while it reaches the maximum around the positions when the two heat capacity flow rates exhibit opposite change trends. The total entransy dissipation decreases and the total exergy efficiency increases with the decrease in the mass flow rate of methanol or the increase in the pressure of  $N_2$ , while the required total heat conductance increases. The heat exchange performance of evaporator improves at the cost of heat conductance. The total entransy dissipation reaches the minimum and the total exergy efficiency achieves the maximum when about 66%, 65% and 61% of the total heat load is undertaken by the low temperature section at the  $N_2$  pressure of 5 MPa, 7 MPa and 9 MPa, respectively. The extractable cold amount from the liquid  $N_2$  in the same temperature rise decreases with the increase in the  $N_2$  pressure.

When the total heat conductance is given, the required mass flow rate of methanol increases with that of propane. As the mass flow rate of propane increases, the required inlet temperature of propane decreases and the outlet temperature of  $N_2$  increases. The local heat capacity rate ratio equals one at several positions along the flow direction of  $N_2$ , where the change trends of local heat transfer rate, local effectiveness and local entransy dissipation are inverted. The minimum total entransy dissipation and the maximum total exergy efficiency can be achieved by adjusting the mass flow rate of propane, while their corresponding mass

flow rates of propane are different. Increasing the pressure of  $N_2$  is beneficial to lessening the minimum entransy dissipation and increasing the maximum exergy efficiency. The affordable heat load or cold amount from the liquid  $N_2$  increases as the mass flow rate of propane increases or the pressure of  $N_2$  decreases. The demands for the outlet temperature of 283 K and low entransy dissipation can be simultaneously satisfied when about 67% of the total heat conductance is distributed to the low temperature section for various pressures of  $N_2$ , while about 69% of the total heat conductance should be distributed to the low temperature section to achieve higher exergy efficiency.

The performance of T- $N_2$  evaporator cannot be intuitively predicted due to drastic variation of thermo-physical properties of  $N_2$  in the transcritical heat exchange process with wide working temperature range and multiple working pressure options. The operating parameters of T- $N_2$  evaporator should be carefully tailored to avoid its invalidation and elevate its overall performance.

## **Acknowledgement**

The authors would like to acknowledge the financial support of the Engineering and Physical Sciences Research Council (EPSRC) of the United Kingdom (Grant Nos. EP/N000714/1 and EP/N021142/1), National Natural Science Foundation of China (Grant Nos. 51606135 and 51776142) and Natural Science Foundation of Hubei Province (Grant No. 2016CFB156).

## References

- [1] B. Ameel, C. T'Joel, K. De Kerpel, P. De Jaeger, H. Huisseune, M. Van Belleghem, M. De Paepe, Thermodynamic analysis of energy storage with a liquid air Rankine cycle, *Applied Thermal Engineering*, 52 (2013) 130-140.
- [2] R. Morgan, S. Nelmes, E. Gibson, G. Brett, Liquid air energy storage – Analysis and first results from a pilot scale demonstration plant, *Applied Energy*, 137 (2015) 845-853.
- [3] X.D. Xue, S.X. Wang, X.L. Zhang, C. Cui, L.B. Chen, Y. Zhou, J.J. Wang, Thermodynamic Analysis of a Novel Liquid Air Energy Storage System, *Physics Procedia*, 67 (2015) 733-738.
- [4] E. Borri, A. Tafone, A. Romagnoli, G. Comodi, A preliminary study on the optimal configuration and operating range of a “microgrid scale” air liquefaction plant for Liquid Air Energy Storage, *Energy Conversion and Management*, 143 (2017) 275-285.
- [5] P. Wojcieszak, J. Poliński, M. Chorowski, Investigation of a working fluid for cryogenic energy storage systems, *IOP Conference Series: Materials Science and Engineering*, 278 (2017) 012069.
- [6] L. Chai, J. Liu, L. Wang, L. Yue, L. Yang, Y. Sheng, H.S. Chen, C.Q. Tan, Cryogenic energy storage characteristics of a packed bed at different pressures, *Applied Thermal Engineering*, 63 (2014) 439-446.
- [7] J.D. McTigue, A.J. White, C.N. Markides, Parametric studies and optimisation of pumped thermal electricity storage, *Applied Energy*, 137 (2015) 800-811.
- [8] R. Morgan, S. Nelmes, E. Gibson, G. Brett, An analysis of a large-scale liquid air energy storage system, *Proceedings of the Institution of Civil Engineers - Energy*, 168 (2015) 135-144.
- [9] A. Sciacovelli, A. Vecchi, Y.L. Ding, Liquid air energy storage (LAES) with packed bed cold thermal storage – From component to system level performance through dynamic modelling, *Applied Energy*, 190 (2017) 84-98.
- [10] Y. Li, H. Cao, S. Wang, Y. Jin, D. Li, X. Wang, Y. Ding, Load shifting of nuclear power plants using cryogenic energy storage technology, *Applied Energy*, 113 (2014) 1710-1716.
- [11] X. She, X. Peng, B. Nie, G. Leng, X. Zhang, L. Weng, L. Tong, L. Zheng, L. Wang, Y. Ding, Enhancement of round trip efficiency of liquid air energy storage through effective utilization of heat of compression, *Applied Energy*, 206 (2017) 1632-1642.
- [12] H. Peng, X. Shan, Y. Yang, X. Ling, A study on performance of a liquid air energy storage system with packed bed units, *Applied Energy*, 211 (2018) 126-135.
- [13] G.L. Guizzi, M. Manno, L.M. Tolomei, R.M. Vitali, Thermodynamic analysis of a liquid air energy storage system, *Energy*, 93 (2015) 1639-1647.
- [14] H. Araki, M. Nakabaru, K. Chino, Simulation of heat transfer in the cool storage unit of a liquid–air energy storage system, *Heat Transfer—Asian Research*, 31 (2002) 284-296.
- [15] D. Dimitrov, A. Zahariev, V. Kovachev, R. Wawryk, Forced convective heat transfer to supercritical nitrogen in a vertical tube, *International Journal of Heat and Fluid Flow*, 10 (1989) 278-280.
- [16] A. Nakano, M. Shiraishi, Piston effect in supercritical nitrogen around the pseudo-critical line, *International Communications in Heat and Mass Transfer*, 32 (2005) 1152-1164.
- [17] P. Zhang, Y. Huang, B. Shen, R.Z. Wang, Flow and heat transfer characteristics of supercritical nitrogen in a vertical mini-tube, *International Journal of Thermal Sciences*, 50 (2011) 287-295.

- [18] P. Stathopoulos, K. Ninck, P.R. von Rohr, Heat transfer of supercritical mixtures of water, ethanol and nitrogen in a bluff body annular flow, *The Journal of Supercritical Fluids*, 70 (2012) 112-118.
- [19] C.C. Negoescu, Y.L. Li, B. Al-Duri, Y.L. Ding, Heat transfer behaviour of supercritical nitrogen in the large specific heat region flowing in a vertical tube, *Energy*, 134 (2017) 1096-1106.
- [20] J.F. Guo, Design analysis of supercritical carbon dioxide recuperator, *Applied Energy*, 164 (2016) 21-27.
- [21] Z.Y. Guo, H.Y. Zhu, X.G. Liang, Entransy—A physical quantity describing heat transfer ability, *International Journal of Heat and Mass Transfer*, 50 (2007) 2545-2556.
- [22] A. Bejan, Exergy analysis, entropy generation minimization, and constructal theory, mechanical engineers' handbook: energy and power. Third Edition, vol. 4, in, John Wiley & Sons, Inc, 2006.
- [23] G. Nellis, S. Klein, Heat transfer, Cambridge University Press, New York, 2009.
- [24] R.K. Shah, D.P. Sekulic, Fundamentals of heat exchanger design, John Wiley & Sons, Inc., Hoboken, 2003.
- [25] Z.Y. Guo, X.B. Liu, W.Q. Tao, R.K. Shah, Effectiveness–thermal resistance method for heat exchanger design and analysis, *International Journal of Heat and Mass Transfer*, 53 (2010) 2877-2884.
- [26] W.H. Wang, X.T. Cheng, X.G. Liang, Entropy and entransy analyses and optimizations of the Rankine cycle, *Energy Conversion and Management*, 68 (2013) 82-88.
- [27] E. Açıkkalp, Entransy analysis of irreversible heat pump using Newton and Dulong–Petit heat transfer laws and relations with its performance, *Energy Conversion and Management*, 86 (2014) 792-800.
- [28] E. Açıkkalp, Entransy analysis of irreversible Carnot-like heat engine and refrigeration cycles and the relationships among various thermodynamic parameters, *Energy Conversion and Management*, 80 (2014) 535-542.
- [29] Y.D. Zhu, Z. Hu, Y.D. Zhou, L. Jiang, L.J. Yu, Applicability of entropy, entransy and exergy analyses to the optimization of the Organic Rankine Cycle, *Energy Conversion and Management*, 88 (2014) 267-276.
- [30] J.F. Guo, X.L. Huai, X.F. Li, J. Cai, Y.W. Wang, Multi-objective optimization of heat exchanger based on entransy dissipation theory in an irreversible Brayton cycle system, *Energy*, 63 (2013) 95-102.
- [31] J.F. Guo, M.T. Xu, The application of entransy dissipation theory in optimization design of heat exchanger, *Applied Thermal Engineering*, 36 (2012) 227-235.
- [32] X.T. Cheng, X.G. Liang, Computation of effectiveness of two-stream heat exchanger networks based on concepts of entropy generation, entransy dissipation and entransy-dissipation-based thermal resistance, *Energy Conversion and Management*, 58 (2012) 163-170.
- [33] Y. Wang, H. Zhang, X. Huai, X. Li, J. Cai, W. Xi, Exergy analysis of LBE-helium heat exchanger in the experimental cooling loop based on accelerator driven sub-critical power system, *Energy Conversion and Management*, 135 (2017) 274-280.
- [34] M.M. Joybari, F. Haghighat, Exergy analysis of single effect absorption refrigeration systems: The heat exchange aspect, *Energy Conversion and Management*, 126 (2016) 799-810.
- [35] V. Martinaitis, G. Streckienė, D. Biekša, J. Bielskus, The exergy efficiency assessment of heat recovery exchanger for air handling units, using a state property – Coenthalpy, *Applied Thermal Engineering*, 108 (2016) 388-397.

- [36] M. Mehdizadeh-Fard, F. Pourfayaz, A simple method for estimating the **irreversibility** in heat exchanger networks, *Energy*, 144 (2018) 633-646.
- [37] P. Dorosz, P. Wojcieszak, Z. Malecha, Exergetic analysis, optimization and comparison of LNG cold exergy recovery systems for transportation, *Entropy*, 20 (2018) 59.
- [38] NIST Chemistry WebBook, The U.S. Secretary of Commerce on behalf of the United States of America. <http://webbook.nist.gov/chemistry/fluid/>.